Switchable bi-stable multilayer magnetic probes for imaging of soft magnetic structures

Tom Wren[1,2], Robb Puttock[1,2], Boris Gribkov[1,3], Sergey Vdovichev[3], and Olga Kazakova[1]

[1]*National Physical Laboratory, Teddington, TW11 0LW, UK*
[2]*Royal Holloway University London, Egham, TW20 0EX, UK*
[3]*Institute for Physics of Microstructures RAS, Nizhny Novgorod 603950, Russia*

ABSTRACT

We present the use of custom-made multilayer (ML) magnetic probes in magnetic force microscopy (MFM) for imaging soft magnetic structures, i.e. nickel submicron disks of different dimensions. One of the main advantages of a custom-made ML probe is that it can be controllably switched between standard (parallel) and low moment (antiparallel) states. We demonstrate that the predicted vortex and stripe domain states in the disks are observed when using the ML probes both in the antiparallel and parallel states. However, while the phase contrast is significantly larger in the parallel state, the images are dominated by strong sample – probe interactions that obscure the image. By comparison of the stripe domain width observed by MFM with the ML probe and those expected from the Kittel model, we show that the resolution of the probe in the AP and P states is ~30 - 40 nm, i.e. of the order of the probe geometrical apex and thus approaching the limit of spatial resolution. The ML probes are further compared to the commercial standard and low moment ones, showing that the quality of images obtained with the ML probe is superior to both commercial probes.

I. INTRODUCTION

Magnetic force microscopy (MFM) is a powerful technique that allows the imaging of some of the smallest magnetic structures. With MFM it is possible to image magnetic features that are typically only tens of nanometers in size [1,2]. To reach the superior resolution value, which is primarily limited by the dimensions of the magnetic probe apex, several state-of-the art approaches have been utilised to fabricate ultra-high resolution MFM probes. Some of the most promising techniques for the high-resolution probe fabrication are based on scanning electron [3,4] or ion beam technologies [5,6] , another method utilises carbon nanotubes [7,8]. A completely different approach uses a thin multilayer (ML) coating (two layers of ferromagnetic material separated by a non-magnetic interlayer), which leads to the existence of a nanoscale magnetically uncompensated region at the probe's apex [9–12]. Only this uncompensated area plays an active role in the MFM probe-sample interaction, because the magnetic material is "effectively localised" near the probe's apex. A similar approach was also used for fabrication of probes for scanning Kelvin probe microscopy, where the electric field was confined near the probe apex, thus significantly increasing spatial resolution in the Kelvin mode [13].

In this letter, we use custom fabricated ML probes consisting of two 15 nm thick Co layers separated by 10 nm Si interlayer, such that the magnetic layers of the probe can be magnetised in either parallel (P) or antiparallel (AP) configuration and can be used in standard or low moment states, dependent on desired application. The ML probes are used to image nickel nanodisks in vortex and stripe domains states. We further utilise theoretical models to predict the limits of the expected magnetic features. Comparisons of MFM observations show that ML probes are superior in numerous ways to commercial ones. Potential applications of the switchable ML probes include but are not limited to: i) studying materials with unknown magnetic properties by adjusting the probe's moment without the need to change the scanning area; ii) evaluation of 'odd' and unexpected magnetic features by consequent imaging in P/AP states; iii) identification and reduction of electrostatic effects; iv) controllable local modification of the sample's domain structure by the probe in the large moment state (e.g. introducing/tracking a domain wall within a magnetic nanowire [14]), followed by imaging in the low moment state. The latter approach is suitable for in-plane magnetised samples but should be used with a care for samples with the out-of-plane magnetization.
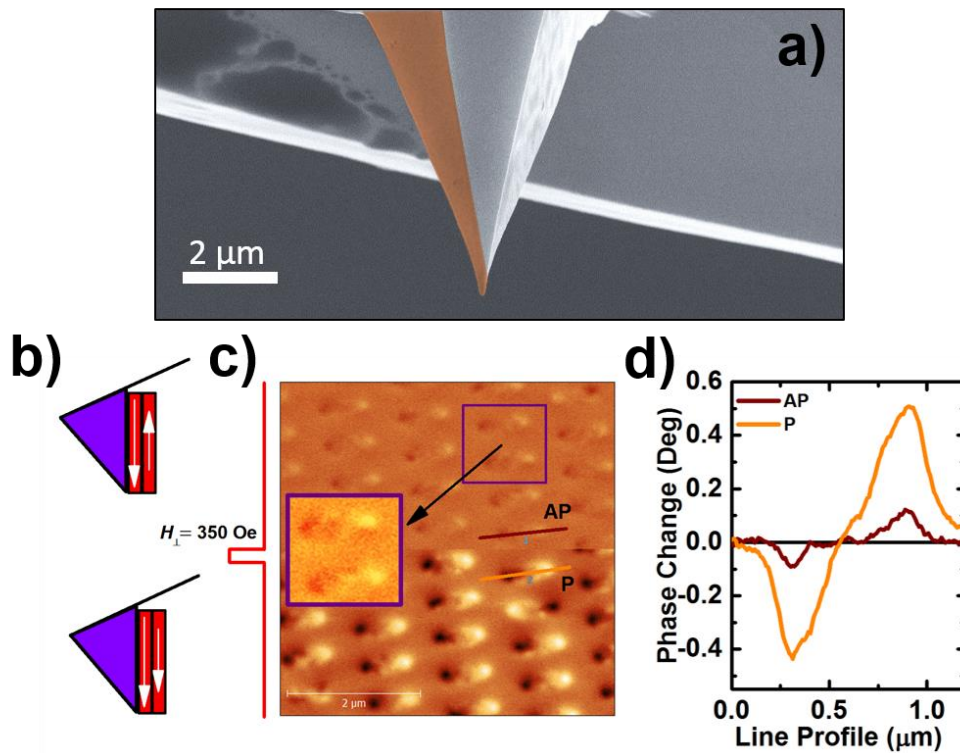
Fig. 1. a) SEM of ML MFM probe with magnetic multilayer on the rear-face of the pyramidal probe highlighted in brown. b) The orientation of the probe's magnetic layers in the AP and P states. c) MFM image of the test sample (an array of FeCr elliptical dots) obtained with ML MFM probe. The probe is initially magnetized in the anti-parallel (AP) state (top half). Half-way through the scan, a pulse of $H_\perp$ = 350 Oe is applied out-of-plane to the sample to switch the probe to the parallel (P) state. Inset: an enhanced image of the FeCr dots emphasizing their complex multi-domain substructure. d) Line profiles of elliptical FeCr dots obtained using a probe magnetized either in the P or AP states.

II. EXPERIMENTAL

We use three types of magnetic probes: 1) commercial standard moment (SM) probes with ~40 nm CoCr magnetic coating, nominal force constant k = 2.8 N/m and resonant frequency f_0 = 75 kHz (MESP, Bruker); 2) commercial low moment (LM) probes with ~15 nm CoCr magnetic coating, k = 3 N/m and f_0 = 70 kHz (Low Moment, NT-MDT); as well as custom-made ML probes, described below.

A series of ML MFM probes has been fabricated in house, using magnetron sputtering technique (AJA International Aurora, ATC-2200, USA) in Ar atmosphere with the residual pressure ~10 −6 Torr. Commercial Si cantilevers (PPP-MFMR, Nanosensors) with typical f_0 = 70–80 kHz, k = 2–3 N/m and curvature radius of ~10 nm have been chosen for coating. To clean the surface before sputtering, the cantilevers were treated by ion etching in Ar atmosphere. The ion etching and thin film sputtering procedures have been done in the connected vacuum chambers without breaking the vacuum level.

The magnetic coating of the ML probe consists of two 15-nm thick Co layers separated by 10-nm thick Si interlayer, where thin film thicknesses were estimated using SEM data and material deposition rates measured on flat surfaces (Fig. 1a). Additionally, thin Cr layers were used both as an adhesion layer and a top layer to protect the ML magnetic structure from oxidation. Due to the pyramidal shape of the probe, the magnetic coating was formed only on the backside of the probe, which is perpendicular to the sample surface during scanning. To create a uniform Si interlayer and avoid interconnection of magnetic layers at the pyramid edges, the sample holder with the mounted cantilevers was rotated during Cr interlayer deposition. The final curvature radius of custom-made probes was estimated to be ~30 nm.

Nickel disk arrays were fabricated using e-beam lithography and lift-off techniques. The two disk arrays have dimensions of 800 nm diameter and 25 nm thickness, and 1000 nm diameter and 45 nm thickness. Nickel was chosen because of its relative magnetic softness, whereas the disk geometry was chosen due to a characteristic vortex state (800 nm diameter, 25 nm thick) or stripe domain state (1000 nm diameter, 45 nm thick) that can be observed in the disks [15–17] , which are both easily recognisable in MFM imaging [17,18]. Additionally, to act as a test sample, an array of elliptical FeCr dots with large coercivity and 280×700 nm dimensions was fabricated [19,20].

Samples were measured using an MFM technique in a two-pass lift mode: the first pass tracks the topography in semi-contact tapping mode with the probe oscillation amplitude of ~20 nm and the second pass retraces the topography at 30 nm above the surface using the same set-point oscillation amplitude. Changes to the cantilever oscillation are therefore due to the action of magnetic forces between the probe and sample. MFM measurements were performed using an NT-MDT NTEGRA Aura scanning probe microscope (SPM), that allows the application of either in-plane or out-of-plane magnetic field in-situ during the measurement.

The MFM response of the test sample with a high magnetic anisotropy and stable configuration of the magnetic states is shown in Fig. 1c. Before taking the image, the sample was saturated in plane ($H_\parallel$ = 3 kOe) along the easy axis of the dots and the majority of the dots were uniformly magnetised in one direction [19]. The patterned structures demonstrate in-plane anisotropy and their magnetic state was not affected by the pulse of the out-of-plane magnetic field ($H_\perp$ = 350 Oe), which was applied in MFM measurements in-situ. To verify this, the same area

3

was scanned with a standard single-layer probe before and after applying the pulse of the out-of-plane field. No changes of magnetisation distribution within the structures were observed, verifying the stability of magnetization of FeCr dots.

Transitions between P and AP magnetic configurations are clearly seen during MFM scanning after the pulse of the vertical magnetic field was applied (Fig. 1c). The upper part of this image was obtained with the AP configuration of the ML probe. In the middle of the scan, a short pulse of out-of-plane magnetic field ($H_\perp$ = 350 Oe) was applied and, finally, the lower part of the scan was obtained with the MFM probe in the P configuration. To switch the ML probe back to the AP configuration, application of only $H_\perp$ = 150 Oe in the reversed direction was needed. Such a large difference in the values of switching magnetic fields is determined by strong magnetostatic coupling between magnetic layers. In the P state, each magnetic layer is affected by the demagnetising magnetic field of another layer, the direction of this field is opposite to the magnetization direction within the layer, thus decreasing the P-AP switching field value. In case of the AP state, magnetic field created by each individual magnetic layer stabilises another layer and this increases the AP-P switching field value [21]. Note that both P and AP magnetic states of the ML MFM probe are stable after removing the field.

It is evident from Fig. 1c and d that the transition from the P to AP configuration leads to: decreasing magnitude of the MFM signal; and localisation of magnetic poles (dark and bright contrasts) near the horizontal vertices of the patterned structures. These domain wall like patterns reveal the additional close domain substructure in the centre of the elliptical dots (Fig. 1c, inset), which is attributed to an increase of lateral resolution [12].

III. Results

First, we used the ML probe to image a nickel disk of diameter 800 nm and thickness 25 nm. Images were taken in two-pass lift mode with the lift height of 30 nm for both the P and AP states. The probe was first magnetised in the P configuration, which was tested using the FeCr dot test sample. The Ni disk was then imaged in the P state (Fig. 2a). A pulse of $H_\perp$ = 350 Oe was then applied to switch the probe to the AP state and the same disk was imaged again (Fig. 2b). Neither the sample nor the probe were removed from the SPM system during this procedure. It is important to note that only magnetisation of the ML MFM probe was affected by the pulse of the out-of-plane field, whereas the switching field of the vortex core has been shown to be about ten times larger than the magnetic fields applied here [22]. Figs. 2c and d show line profiles taken in the top (solid line) and central (dashed line) parts of the disk, respectively

In the P probe configuration (Fig. 2a), fractured radial domains were observed, as well as the magnetic stray field outside of the physical boundary of the disk. In the AP probe configuration (Fig. 2b), a clear vortex core can be seen in the centre of the disk as a bright contrast spot. Some magnetic contrast is also seen in the z-plane of the disk, yet with a magnitude comparable with that of the background signal, i.e. only several tenths of a degree. The line profiles through the top of the disk reveal stark differences between the P and AP states (Fig. 2c). While the AP state shows the expected near zero response in the plane of the disk, the P state demonstrates an appreciable difference in the phase shift between the disk and background as well as extra domains and domain wall like

features, e.g. in the top right part of the disk. The line profile taken through the vortex core in the AP state (Fig. 2d) clearly shows the core as a peak in the phase shift. The core size is ~100 nm, which is much larger than the typically quoted value of 10 nm in Py disks [23]. In the P state, the core has a size of ~400 nm, i.e. even greater than that in the AP state. The core position also appears off-centre in the P state compared to the AP one. The large core size can be attributed to two factors: 1) magnetocrystalline anisotropy [24] - the core in nickel is significantly larger than in permalloy disks due to its larger out-of-plane anisotropy [17]; 2) the convolution of the actual core size and the finite size of the probe apex. Furthermore, the effective size of the magnetic moment will be larger in the P state than for AP, explaining the discrepancy in the measured core sizes between the two scans.
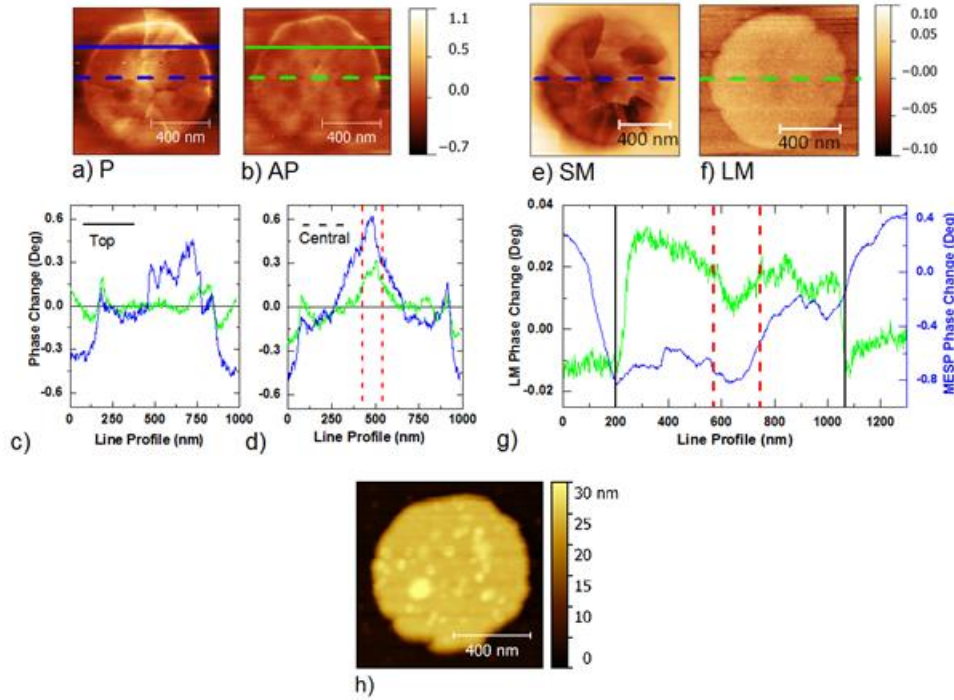
Fig. 2. MFM images of a nickel disk (diameter 800 nm and thickness 25 nm) measured with a custom-made ML probe in the a) P and b) AP states as well as commercial probes with e) standard and f) low moments. Orientation of the probes are arbitrary. The line profiles extracted from P and AP states for c) top (solid line) and d) central (dashed line) cross-sections indicate the phase change due to the nickel disk's domain structure. The green/blue lines are for the AP/P states, respectively. The vertical red dashed lines in d) mark the core size in the AP state. g) The line profiles (green and blue lines) obtained with LM and SM commercial probes, respectively. Black solid lines show the geometrical size of the Ni disk and red dashed lines mark the outline of the vortex core measured by the LM probe. The LM/SM commercial probes show a similar response to the ML probe in the AP/P states. Magnetic orientation of the probes is arbitrary. The topography of the Ni disk obtained by the custom-made probe (h) is included for reference.

The measured core sizes can be compared to the expected core diameter ($2r_{core}$), which can be estimated using the equation derived by Garcia et al. [24]:

$$2r_{core} = 2\sqrt{\frac{A}{K_d - K_z}} \qquad (1)$$

5

where $A = 9 \times 10^{-12}$ Jm^{-1} is the exchange constant of Ni; $K_d = \frac{1}{2}\mu_0 M_s^2$ is the magnetostatic energy density; and K_z is the effective out-of-plane anisotropy. By using $K_z = 7.2 \times 10^4$ Jm^{-3}, as has been previously shown to be appropriate for nickel disk of this thickness [17] and assuming saturation magnetization of $M_s \approx 347$ kAm^{-23}, we obtain the core diameter of ~100 nm. This is a close match to an experimental value as observed using ML probes in the AP state, indicating that the resolution of the AP state is comparable (or better) to the real core size, such that the convolution of the probe apex and core does not significantly affect the measurements.

We further compared the images of the vortex state obtained with the ML probe with ones measured from commercial standard moment (SM) and low moment (LM) probes, Fig. 2e and f, respectively. The image obtained with a SM probe shows a fractured, radial domain structure similar to that of the ML probe in the P state. Alternatively, the LM probe demonstrates a smooth response comparable with the AP state of the ML probe, but with much reduced contrast. Corresponding line profiles of MFM images taken through the same area of the disk are compared in Fig. 2g. The SM probe response is about 10 times larger than that of the LM probe. Both the LM and SM commercial probes detect a core like structure, as would be expected in a vortex state [18], as a trough in the line profile at the disk centre. However, the SM line profile shows additional abrupt changes of magnetisation associated with the fractured domain wall structure. Furthermore, the SM probe appears to interact with the disk magnetisation outside the area of the disk, manifesting as threads of magnetic response that continue out of the disk from the domain wall structures.

The difference between Fig. 2e and f is attributed to the interaction between the probe and sample during the scan. In the case of the LM probe (Fig. 2f), the magnetisation of the vortex is not affected by the magnetic moment of the probe. As such, the core of the vortex can be observed as a faint dark spot and the MFM response is minimal in the plane of the disk, as expected [18]. The SM probe (Fig. 2e), which has an out-of-plane magnetic moment, strongly interacts with the sample; causing the magnetisation of the sample to be pulled out-of-plane as the probe scans. This is evident by the strong dark contrast in the disk, as well as the fractured domain structure. Previously such probe-sample interactions were investigated through the use of force dissipation microscopy [25–27], where the energy dissipated by the cantilever was calculated, and this information was further used to determine the probe-sample interaction. Additionally, the bright contrast of the main part of the disk could be attributed to the effect of the electrostatic forces, as in this case the magnetic interaction between the LM probe and in-plane magnetisation of the disk is minimal.

By comparison of the images obtained by ML and commercial probes, it is clear that the ML probe in its P state behaves much like a commercial SM probe, whereas the AP state is similar to a LM probe. However, the ML probe has certain advantages over both commercial probes. In the P state, the ML probe still shows the radial domain like structure due to strong interaction between the probe and sample, yet to a much lesser degree than the standard moment commercial probe. As such, the P state ML probe is more suited than the commercial probe for measuring soft materials, while still producing an apprehensible contrast. The greatest advantage of the ML probe, however, is in the AP state. Fig. 2f signifies that to accurately measure the magnetic states of the soft nickel a low moment probe must be used. However, the maximum phase change obtained with the commercial LM probe is only 0.1°, while the phase change due to the core is only 0.01°. This makes interpretation of the images very difficult. At the

same time, the phase change of the core measured with the AP state is 0.3°, i.e. 30 times greater than that of the LM probe, while the disk magnetic state remains unaffected by the probe. We further compare the spatial resolution of the LM probe and the ML probe in the AP state by comparing the measured sizes. The core size observed using the LM probe is ~180 nm, i.e. almost twice as large as that observed using the AP state, indicating that for the former probe the convolution effect is not negligible. This specifies that the AP state has better spatial resolution than LM probe. These observations demonstrate that the custom-made ML probes in the AP state are superior for imaging of soft magnetic structures.
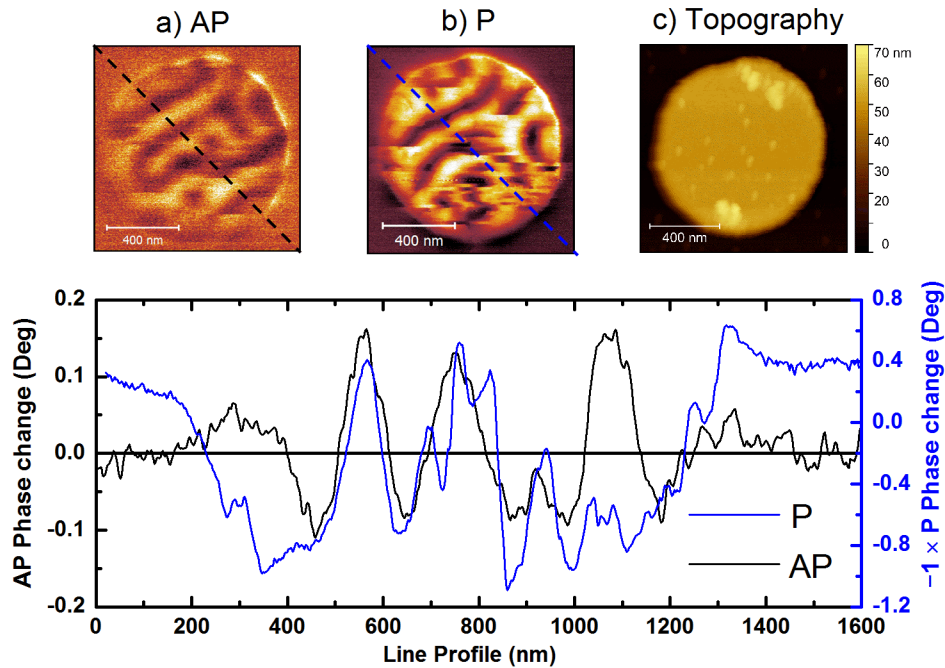
Fig. 3. MFM images of a nickel disk (diameter 1000 nm and thickness 45 nm) as measured with an ML probe in the AP (a) and P (b) states. AP and P states have opposite magnetization orientation. The topographic image of the nickel disk (c) measured by the ML probe is included as reference. The line profiles of the nickel disk obtained by the ML probe in AP and P states (black and blue, lines respectively) are compared in (d). In both states, the stripe domain width is ~70 nm. However, the P state shows multiple switching of magnetization, *e.g.* in the bottom half of the disk, is due to strong probe-sample interaction.

We demonstrate the advantages of the ML probe in the AP state further by imaging a larger and thicker nickel disk (diameter 1000 nm and thickness 45 nm) which has a remnant stripe domain state [17]. The MFM images obtained with the AP/P states of the ML probe are shown in Figs. 3a and b respectively, alongside the topographical image (Fig. 3c), with the diagonal line profiles of each image compared in Fig. 3d. Images were taken with opposite probe magnetizations because, when applying the magnetic pulse to switch from the P to AP state, it is difficult to predict which layer will switch. Hence, the line profile of the P state is inverted in Fig 3d for comparative purposes. It is noteworthy that some domains (i.e. top left and bottom right) in Fig. 3b appear to be shifted compared to the initial image in Fig. 3a. This is probably an artefact of the sample – probe interaction occurring when the sample is scanned with the ML probe in the P state. Besides this, the positions of the striped domains match in the center of the disk for both magnetic states of the probe, evident by the well-aligned troughs/peaks (e.g. peak at ~550 nm in

Fig. 3d). Beyond ~875 nm in the line profile the phase for the probe in the P state starts to deviate from the equivalent line profile for the AP state. This is from magnetic switching in the bottom half of the disk, as indicated by abrupt horizontal lines, across which the phase contrast changes sign (Fig. 3b). The P state demonstrates a range of ~1.5 degrees for the phase change, while for AP it is just ~0.25 degrees. In both P and AP states, the stripe domain period is resolved to be ~70 nm.

The resolution of the probes can be tested by comparing the measured stripe domain width to the expected one, which can be calculated by using Kittel's theory [28]. We chose to use this model as presented by Virot et al. [29] as it expresses all spatial values in units of $\sqrt{A/K}$, such that:

$$\tilde{t} = t/\sqrt{A/K} \quad \tilde{d} = d/\sqrt{A/K} \tag{2}$$

where t is the thickness of the film, d is the stripe domain width, while $\tilde{t}$ and $\tilde{d}$ denote the same values in units of domain wall width. By energy minimization, the stripe domain width is thus:

$$d = 3.84\sqrt{\frac{A}{K}}\sqrt{Q\tilde{t}} \tag{3}$$

$$Q = \frac{2K_z}{\mu_0 M_s^2} \tag{4}$$

where Q is the dimensionless quality ratio of the out-of-plane anisotropy (K_z) to the magnetostatic energy density. We consider $K_z = 8.1 \times 10^4$ Jm^{-3}, as was shown to be appropriate for nickel disks of this thickness [17], and $M_s = 347$ kAm^{-1} and 490 kAm^{-1} for the respective lower and upper bounds of the saturation magnetization. Here, the lower bound was used to fit to the observed core size in Ni dots with vortex structures and the upper bound value denoted the bulk saturation magnetization of nickel. Thus, the stripe domain period (d) is calculated to be in the range of 60 – 87 nm for the respective upper and lower bounds of M_s. The observed stripe domain width of 70 nm is comfortably inside this range, indicating a reduced anisotropy constant as compared to the bulk value of nickel. Therefore, the resolution of the ML probes must be at least half of this value to resolve the stripe domains so clearly, giving a resolution of 30 – 43 nm, *i.e.* in the order of the probe apex (radius ~30 nm) and therefore approaching the limit of spatial resolution.

IV. Conclusions

The magnetic state of nickel disks of different dimensions was studied using custom fabricated ML probes, in which the magnetic configuration can be switched between standard (P) and low (AP) moment states and compared with the results obtained from commercial standard and low moment probes.

The strong magnetic moment in the P state exhibits sample–probe interactions similar to the SM probe but with a reduced strength, while retaining the strong magnetic contrast. The probe –sample interactions leading to remagnetisation of individual domains are not observed in the AP state, i.e. similar to the commercial LM probe, but with a much greater magnetic contrast. By imaging a stripe domain disk and comparing the observed width of the stripe domains with the theoretically expected value, we show that the lateral resolution of the probes is in the range

of 30– 43 nm. This resolution is in the order of the probe apex, thus approaching the limit of possible spatial resolution. Hence, the homemade ML probes demonstrate clear advantages against the commercial ones:

- Switchable magnetic moments without the need to remove the probe away from the SPM system, allowing flexibility for the MFM operator's requirements; an option not offered by common probe manufacturers.

- Higher lateral resolution (in the AP state) than the commercial equivalents.

- Numerous practical applications, including i) study of materials with unknown magnetic properties [30]; ii) evaluation of unknown magnetic features by consequent imaging in P/AP states [31]; iii) identification and reduction of electrostatic effects [32]; iv) controllable local modification of the sample's domain structure by the probe in the P state followed by imaging in the AP state [33].

- Relatively simple to manufacture the switchable probes in industrial conditions, i.e. without involvement of any additional processes, and increase of the production cost compare to the current commercial probes.

V. Acknowledgements

1. Koblischka, M. R. & Hartmann, U. Recent advances in magnetic force microscopy. *Ultramicroscopy* **97,** 103–112 (2003).

2. Belova, L. M., Hellwig, O., Dobisz, E. & Dan Dahlberg, E. Rapid preparation of electron beam induced deposition Co magnetic force microscopy tips with 10 nm spatial resolution. *Rev. Sci. Instrum.* **83,** 93711 (2012).

3. Utke, I., Hoffmann, P., Berger, R. & Scandella, L. High-resolution magnetic Co supertips grown by a focused electron beam. *Appl. Phys. Lett.* **80,** 4792–4794 (2002).

4. Tay, A. B. H. & Thong, J. T. L. Fabrication of super-sharp nanowire atomic force microscope probes using a field emission induced growth technique. *Rev. Sci. Instrum.* **75,** 3248–3255 (2004).

5. Phillips, G. N., Siekman, M., Abelmann, L. & Lodder, J. C. High resolution magnetic force microscopy using focused ion beam modified tips. *Appl. Phys. Lett.* **81,** 865–867 (2002).

6. Amos, N. *et al.* High-resolution and high-coercivity FePtL1[sub 0] magnetic force microscopy nanoprobes to study next-generation magnetic recording media. *J. Appl. Phys.* **105,** 0–3 (2009).

7. Kuramochi, H. *et al.* A magnetic force microscope using CoFe-coated carbon nanotube probes. *Nanotechnology* **16,** 24–27 (2004).

8. Wolny, F. *et al.* Iron filled carbon nanotubes as novel monopole-like sensors for quantitative magnetic force microscopy. *Nanotechnology* **21,** 435501 (2010).

9. Oti, J. O., Rice, P. & Russek, S. E. Proposed antiferromagnetically coupled dual-layer magnetic force microscope tips. *J. Appl. Phys.* **75,** 6881–6883 (1994).

10. Casey, S. M., Lord, D. G., Grundy, P. J., Slade, M. & Lambrick, D. Single layer and multilayer tip coatings in magnetic force microscopy. *J. Appl. Phys.* **85,** 5166 (1999).

11. Wu, Y., Shen, Y., Liu, Z., Li, K. & Qiu, J. Point-dipole response from a magnetic force microscopy tip with a

synthetic antiferromagnetic coating. *Appl. Phys. Lett.* **82,** 1748–1750 (2003).

12. Amos, N., Ikkawi, R., Haddon, R., Litvinov, D. & Khizroev, S. Controlling multidomain states to enable sub-10-nm magnetic force microscopy. *Appl. Phys. Lett.* **93,** 203116 (2008).

13. Brown, K. a, Satzinger, K. J. & Westervelt, R. M. High spatial resolution Kelvin probe force microscopy with coaxial probes. *Nanotechnology* **23,** 115703 (2012).

14. Corte-León, H. *et al.* Anisotropic magnetoresistance state space of permalloy nanowires with domain wall pinning geometry. *Sci. Rep.* **4,** 6045 (2014).

15. Cowburn, R. P., Koltsov, D. K., Adeyeye, A. O. & Welland, M. E. Single-Domain Circular Nanomagnets. *Phys. Rev. Lett.* **83,** 1042–1045 (1999).

16. Skidmore, G., Kunz, A., Campbell, C. & Dahlberg, E. Micromagnetic domain structures in cylindrical nickel dots. *Phys. Rev. B* **70,** 12410 (2004).

17. Wren, T., Gribkov, B., Petrashov, V. & Kazakova, O. Phase diagram of magnetic states in nickel submicron disks. *J. Appl. Phys.* **118,** 23906 (2015).

18. Shinjo, T. Magnetic Vortex Core Observation in Circular Dots of Permalloy. *Science (80-.).* **289,** 930–932 (2000).

19. A. M. Alekseev *et al.* Observation of laser-induced local modification of magnetic order in transition metal layers. *J. Exp. Theor. Phys. Lett.* **73,** 192–196 (2001).

20. Alexeev, A., Bykov, V. A., Popkov, A. F., Polushkin, N. I. & Korneev, V. I. Remanent state studies of elliptical magnetic particles. *J. Magn. Magn. Mater.* **258–259,** 42–44 (2003).

21. Worledge, D. C. Magnetic phase diagram of two identical coupled nanomagnets. *Appl. Phys. Lett.* **84,** 2847–2849 (2004).

22. Okuno, T., Shigeto, K., Ono, T., Mibu, K. & Shinjo, T. MFM study of magnetic vortex cores in circular permalloy dots: Behavior in external field. *J. Magn. Magn. Mater.* **240,** 1–6 (2002).

23. Betto, D. & Coey, J. M. D. Vortex state in ferromagnetic nanoparticles. *J. Appl. Phys.* **115,** 17D138 (2014).

24. Garcia, F. *et al.* Tailoring magnetic vortices in nanostructures. *Appl. Phys. Lett.* **97,** 22501 (2010).

25. Cleveland, J. P., Anczykowski, B., Schmid, A. E. & Elings, V. B. Energy dissipation in tapping-mode atomic force microscopy. *Appl. Phys. Lett.* **72,** 2613 (1998).

26. Moreland, J. Magnetic dissipation force microscopy studies of magnetic materials. **83,** 7333–7338 (1998).

27. Bates, J. R., Miyahara, Y. & Asenjo, A. Tip-induced artifacts in magnetic force microscopy images Oscar. **22417,** 2–5 (2013).

28. Kittel, C. Theory of the Structure of Ferromagnetic Domams in Films and Small Particles. *Phys. Rev.* **70,** (1946).

29. Virot, F., Favre, L., Hayn, R. & Kuz'min, M. D. Theory of magnetic domains in uniaxial thin films. *J. Phys. D. Appl. Phys.* **45,** 405003 (2012).

30. Vock, S. *et al.* Magnetic vortex observation in FeCo nanowires by quantitative magnetic force microscopy. *Appl. Phys. Lett.* **105,** (2014).

31. Kuramochi, H. *et al.* Advantages of CNT-MFM probes in observation of domain walls of soft magnetic materials. *Surf. Sci.* **601,** 5289–5293 (2007).

32. Cambel, V. *et al.* Magnetic elements for switching magnetization magnetic force microscopy tips. *J. Magn. Magn. Mater.* **322,** 2715–2721 (2010).

33. Zhu, X., Grütter, P., Metlushko, V. & Ilic, B. Magnetic force microscopy study of electron-beam-patterned soft permalloy particles: Technique and magnetization behavior. *Phys. Rev. B - Condens. Matter Mater. Phys.* **66,** 244231–244237 (2002).